ISSN (Print) 1226-1750
ISSN (Online) 2233-6656
Journal of Magnetics 18(4), 487-493 (2013) http://dx.doi.org/10.4283/JMAG.2013.18.4.487

Development of Wound Rotor Synchronous Motor for Belt-Driven e-Assist System

Geun-Ho Lee*, Heon-Hyeong Lee, and Qi Wang

Graduate School of Automotive Engineering, Kookmin University, Seoul 136-702, Korea

(Received 15 October 2013, Received in final form 22 November 2013, Accepted 25 November 2013)

The automotive industry is showing widespread interest in belt-driven electric motor–assisted (e-Assist) systems. A belt-driven assist system (BAS) starts and assists the combustion engine in place of the conventional generator. In this study, a water-cooled wound rotor synchronous motor (WRSM) for the e-Assist system was designed and analyzed. The performance of the WRSM was compared with that of an interior permanent magnet synchronous motor (IPMSM). The WRSM efficiency can be improved for the BAS by adjusting the field flux at high speeds. The field current map to obtain the maximum efficiency based on the speed and torque was developed. To control the field flux via field current control in the WRSM, a general H-bridge circuit was added to the WRSM inverter to get the rapid current response in the high-speed region; the characteristics were compared with the chopper circuit. A WRSM developed for the belt-driven e-Assist system and a prototype 115 V power electronic converter to drive the WRSM were tested with a 900 cc combustion engine. The test results showed that the WRSM-type e-Assist system had good characteristics and could successfully start and assist the 900 cc combustion engine.

Keywords: e-Assist system, wound rotor synchronous motor, integrated starter and generator, PWM inverter

1. Introduction

The belt-driven assist system (BAS) is gaining attention for use in mild hybrid electric vehicles (HEVs). The idle stop and go function of the BAS is important in areas with heavy traffic such as urban streets. Idle stop ceases engine operation in order to eliminate fuel consumption and emissions when the vehicle stops temporarily. After an idle stop, the engine is restarted automatically by the BAS motor. A BAS increases the vehicle fuel economy and comprises an electric machine, power electronics, a controller, and a 115 V battery. Using belt-driven e-Assist (electric motor–assisted) systems was found to improve the fuel economy of vehicles by more than 10% when driving in the city [1, 2].

Because replacing the 12 V DC generator mounted on the combustion engine with the BAS allows the conventional engine room structure to be retained, many automotive engineers are interested in adopting the BAS.

The belt-driven e-Assist system provides starting, generating, torque-assisting, and three-phase pulse-width modulation (PWM) converter functions for regenerative braking [2, 3]. During starting mode, the machine operates at low speed and is self-driven with torque control; it operates at maximum torque for sufficiently fast cranking. In generating mode, the converter can operate in synchronous rectifier mode or three-phase PWM converter mode with the torque regulation function [3, 4].

Electric machines currently employ drives based on permanent magnet synchronous motors (PMSMs) or induction motors for BAS. Induction motors and PMSMs can be driven with a proper power electronic converter. These kinds of drives can only reach very high torque at low speeds through the injection of very high current in the machine stator windings. Electromagnetic flux control methodology must be used to drive the motor at very high speeds. PMSM motors are widely adopted in electric and hybrid vehicles. However, the cost is very expensive because of the permanent magnet, and the efficiency is reduced at high speeds owing to the weakened flux. For induction motors, flux control can be adopted at high speeds; however, guaranteeing high torque at low speed is difficult.

Recently, the wound rotor synchronous motor (WRSM) has received a great deal of attention for automotive applications requiring robustness and high-speed operation. It is a cost-effective motor that does not use permanent

*Corresponding author: Tel: +82-2-910-4721
Fax: +82-2-910-4718, e-mail: motor@kookmin.ac.kr

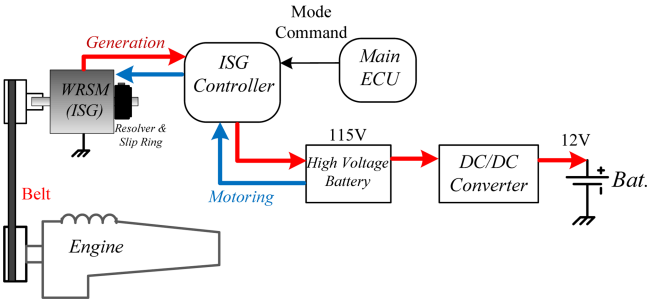

Fig. 1. (Color online) Structure of belt-driven e-Assist system with WRSM.

magnets.

In this study, a WRSM for a belt-driven e-Assist system was developed, as shown in Fig. 1, and compared with an interior permanent magnet synchronous motor (IPMSM). A prototype 115 V power electronic converter to drive the WRSM was developed and tested with a combustion engine. Field control in the WRSM was found to be very important to change speeds rapidly and protect the power electronics; the H-bridge circuit was compared to the chopper circuit for field control. A 900 cc combustion engine with the WRSM prototype was tested and analyzed.

2. Design of Wound Rotor Synchronous Motor for Belt-driven e-Assist System

2.1. Structure of Wound Rotor Synchronous Motor

The WRSM takes the place of the traditional generator and starter and is located where the generator should be. Fig. 2 presents the structure of a water-cooled WRSM. The resolver detects the rotor position, and the slip ring supplies power to the rotor winding. Although the slip ring increases the total volume of the WRSM, it can adjust the amplitude of the rotor flux to maintain a large flux in the low-speed high-torque region and a small flux in the high-speed region. Therefore, the motor operates efficiently at high speeds.

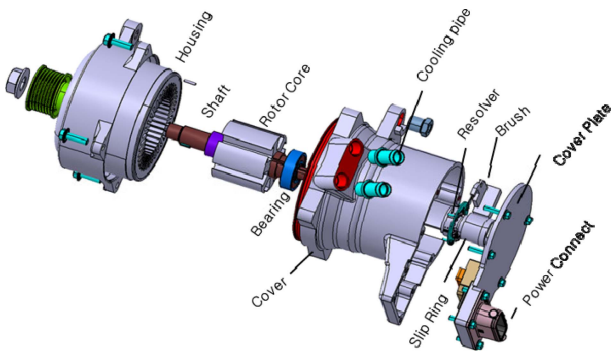

Fig. 2. (Color online) Structure of wound rotor synchronous motor.

Table 1. Design specifications of BAS.

Items	Value
Cold starting WRSM torque	27 Nm
Max. starting current	71 A
Battery voltage	115 V
Max. WRSM speed	9000 rpm
Max. generating power	4 kW
WRSM/engine rpm ratio	2.5
Combustion engine	900 cc

The power circuit for the proposed BAS is a three-phase voltage source inverter that uses an insulated-gate bipolar transistor (IGBT); an H-bridge converter (step-down) is installed to excite the field winding. Feedback signals such as current and voltage are acquired and used by the motor control unit (MCU) with a signal conditioning circuit. The maximum starting torque and generating speed were designed to be 27 N-m and 9000 rpm; the WRSM prototype and controller were combined with a 900 cc combustion engine. Table 1 shows the system specifications of the BAS. The reduction ratio between the WRSM and combustion engine was set to 2.5.

2.2. Design of Wound Rotor Synchronous Motor

The outer dimensions of the motor should be determined for installation with the 900 cc combustion engine; Fig. 3 shows the shape design of the iron core for the stator and rotor. The rotor core of the IPMSM is shown in Fig. 3c [6, 7]. The six poles, 48 V BEMF effective value at 1000 rpm, and 9000 rpm maximum speed motor were designed for high-speed operation based on a maximum available voltage of 115 V from the battery. Table 2 presents other design specifications of the WRSM for the

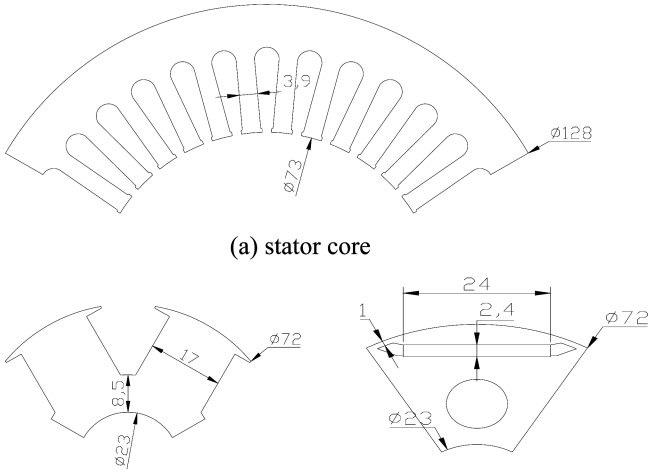

Fig. 3. Designed core shape of WRSM and IPMSM.

Table 2. Design specifications of WRSM.

Items	Value
Stator outer dia./stack length	Φ128/60 mm
Air gap	0.5 mm
EMF @ max. field current	48 Vrms@1000 rpm
Stator resistance	3.6 m
Inductance Ld/Lq @max. field Current	0.33/0.42 mH
Number of stator turns	36 turns
Number of poles	6
Turns of field winding	200 turns
Resistance of field winding	20 Ω

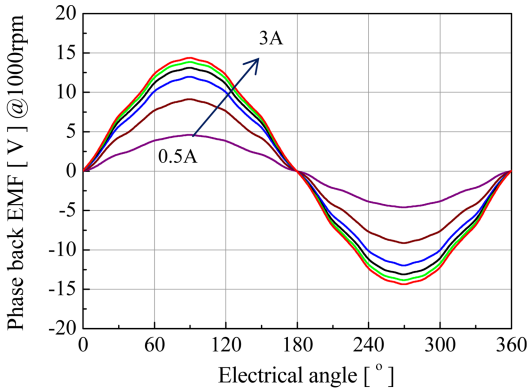

(a) Phase back EMF according to field current [0.5 A → 3 A].

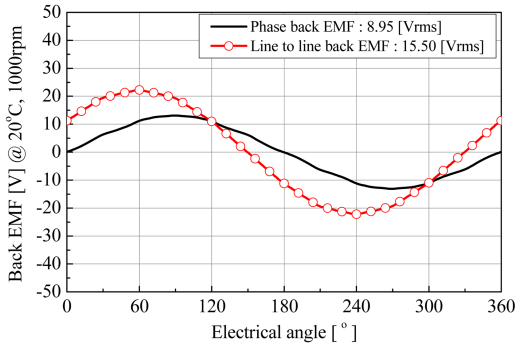

(b) Back EMF wave @ 1.2 A field current

Fig. 4. (Color online) Electromagnetic field analysis results of WRSM.

BAS.

Fig. 4 shows the analysis results for the designed motor. The flux densities of the stator and rotor iron were 1.2T and 1.12 T, respectively, and a 15.5 V line voltage at 1000 rpm was acquired with the 1.2 A field current. Fig. 5 shows that the maximum efficiency was 93.3% under the same conditions.

2.3. Comparison of IPMSM with WRSM

An IPMSM was also designed for comparison with the WRSM. Table 3 presents the characteristics of the WRSM

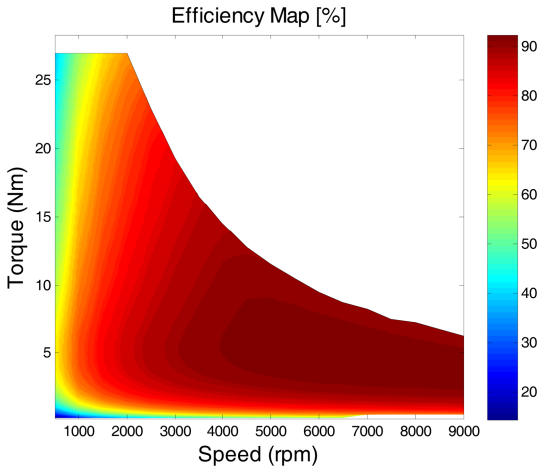

(a) WRSM

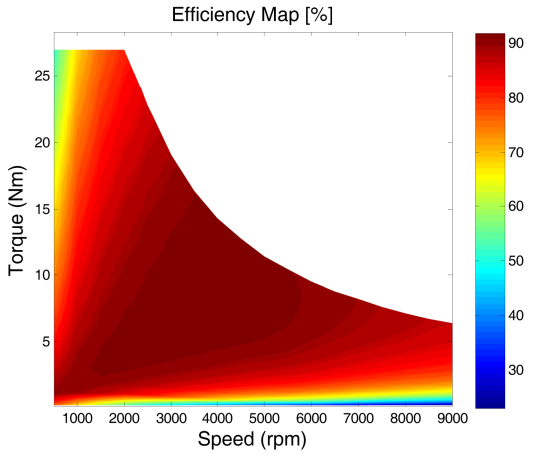

(b) IPMSM

Fig. 5. (Color online) Efficiency map of designed WRSM and IPMSM.

Table 3. Comparison between WRSM and IPMSM.

	Max. power @2150 rpm		Max. power @9000 rpm	
	WRSM	IPMSM 60/50 mm	WRSM	IPMSM 60/50 mm
Torque [Nm]	18	18	4.30	4.30
Power [W]	4053	4053	4053	4053
Phase current	68.2	60.5/73.3	34.02	43.2/39.6
Current ang. [°]	−5.0	37.4/40.8	40.36	75.9/70.5
Field current [A]	2.0	–	1.1	–
Efficiency [%]	80.2	87.1/83.6	89.72	84.5/85.4
Line voltage [rms]	48.1	50.7/44.3	77.25	77.3/77.3
Power factor [%]	82.8	87.7/86.1	97.49	85.2/71.1

and IPMSM. The WRSM had a stack length for the stator core of 60 mm, and the IPMSM had stack lengths of 60 or 50 mm. When the lengths were identical, the IPMSM was approximately 7% more efficient when operating in

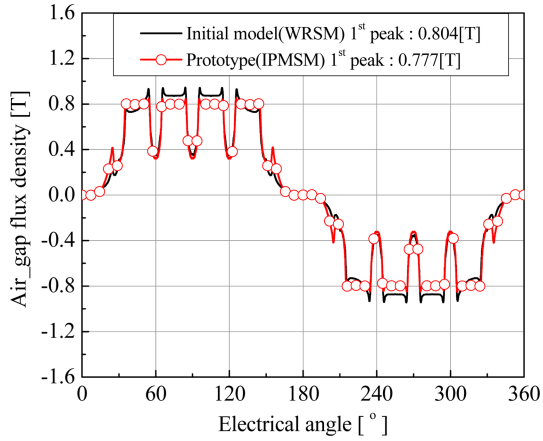

Fig. 6. (Color online) Comparison of air gap flux densities for WRSM and IPMSM (rotor structure of Fig. 3(c)).

the maximum torque region. At maximum speed, the WRSM was 5% more efficient than the IPMSM. Consequently, the WRSM demonstrated good efficiency for frequent high-speed operation. Fig. 6 shows that the WRSM had a higher air-gap flux density than the IPMSM.

3. WRSM Prototype and Experimental Results

3.1. WRSM Prototype and Controller

A water-cooled WRSM prototype was manufactured to study the torque characteristics and the starting and generating functions. The WRSM machine was designed to assist with torque at 6000 rpm and operate at 9000 rpm in generating mode. The controller had an MCU of MPC5643L (Freescale Co.), IGBT with 200 A/600 V (Infineon Co.), and a 470 μF film capacitor for the DC bus. Fig. 7 shows the WRSM prototype with its rotor, and Fig. 8 shows the controller.

3.2. Maximum Efficiency Control of WRSM

In this study, a control method for the WRSM is proposed to improve the main operation efficiency. In general, the current and current vector can be controlled by a

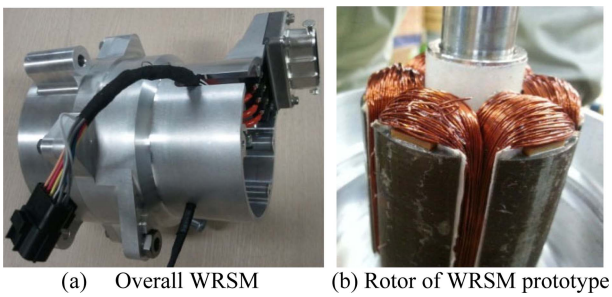

(a) Overall WRSM (b) Rotor of WRSM prototype

Fig. 7. (Color online) WRSM prototype (Max. 9000 rpm).

Fig. 8. (Color online) Controller of WRSM prototype (DC bus voltage: 115 V).

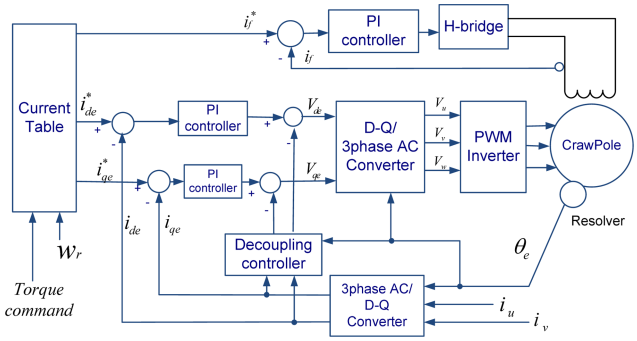

Fig. 9. (Color online) Block diagram for WRSM control.

current feedback control with an inverter. Therefore, all of the motor characteristics can be clearly represented with the current vector. One of the advantages of the WRSM is that controlling the magnetic flux also changes the field current. In addition, the WRSM can be controlled to reduce the magnetic flux at high-speed region rather than applying flux weakening, which widens the controllable region. As EV traction motors operate at high speeds, the WRSM allows a wider range of current vector control compared to the IPMSM [5]. Fig. 9 shows the field current control and control scheme. The field coil inductance is extremely large due to the many coil turns. Therefore, the conventional H-bridge circuit has excellent characteristics for controlling the field current to achieve a fast response performance.

In this study, a control algorithm was adopted that operates at the point of minimum loss – i.e., point of maximum efficiency – based on the changes in i_a and i_f.

$$\begin{aligned} T_m &= P_n[(\Psi_f \times i_{qe}) + (L_d - L_q) \times i_{qe} i_{de}] \\ &= P_n[(\Psi_f \times i_a \cos\beta) + (L_d - L_q) \times i_a^2 \sin 2\beta] \\ &= P_n[(L_f \times i_f \times i_a \cos\beta) + (L_d - L_q) \times i_a^2 \sin 2\beta] \end{aligned} \quad (1)$$

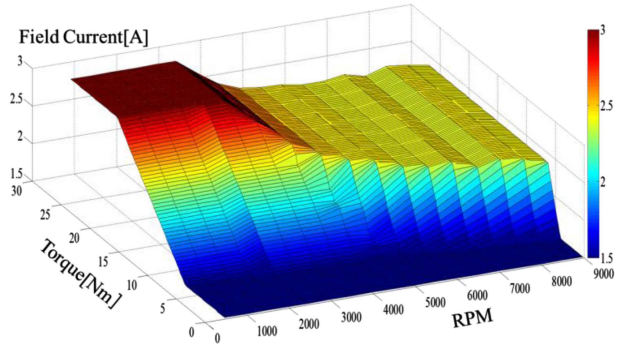

Fig. 10. (Color online) Field current map according to speed and torque.

$$\frac{T_m}{P_n \times i_a} = L_f \times i_f \times \cos\beta + (L_d - L_q) \times i_a \sin 2\beta \quad (2)$$

$$i_f = \frac{1}{L_f \times \cos\beta}\left[\frac{T_m}{P_n \times i_a}(L_d - L_q) \times i_a \sin 2\beta\right] \quad (3)$$

$$W_c = i_a^2 R_a + i_f^2 R_f \quad (4)$$

where Ψ_f is the rotor flux, T_m is the torque, i_{qe} is the q-axis current, i_{de} is the d-axis current, i_a is the phase current, i_f is the field current, L_f is the field inductance, P_n is the pole pair, and L_d, L_d are the stator inductances.

Equations (1) and (2) represent the relationship between the stator current and magnetic flux at the same torque level. Eq. (4) expresses the sum of the stator copper losses and field copper losses, or the total copper losses of the WRSM. In the WRSM, iron losses do not have as much influence as the copper losses and were thus disregarded. i_a and i_f can be determined with the same torque and minimum losses by examining the changes in the speed and torque. Fig. 10 shows the field current map according to the speed and torque.

3.3. Field Current Control of WRSM

In general, a chopper circuit is adopted for field current control of the WRSM. Since the current can only flow in one direction, the negative voltage cannot be used while the field current is turned off, which slows the response speed in the chopper circuit. In the belt-driven e-Assist system, the motor speed change is very quick. Therefore, field flux control of the WRSM is critical, and the response to the field current must be rapid. Consequently, a negative voltage can be applied using the H-bridge topology so that the field current is conditioned rapidly according to the speed. The field current control characteristics were compared for the chopper and H-bridge circuits. Fig. 11 shows the performance according to the control mode. When the field current reference was commanded to go

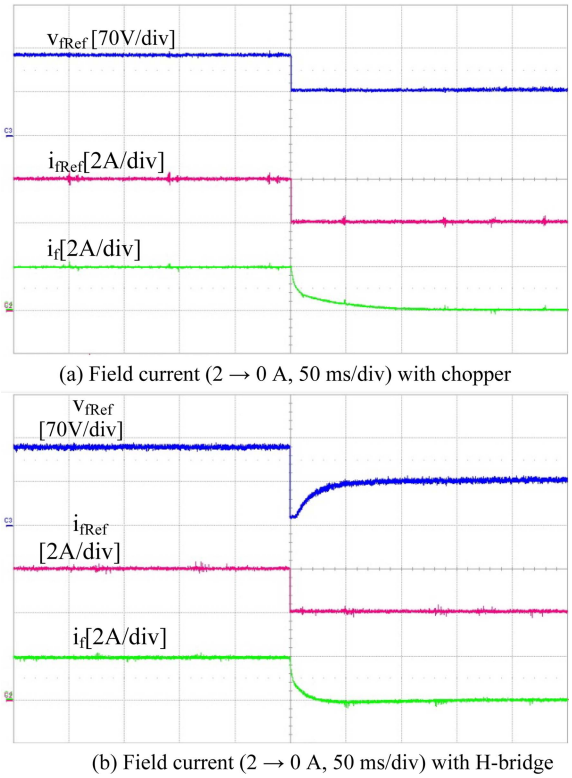

Fig. 11. (Color online) Comparison of field current control methods.

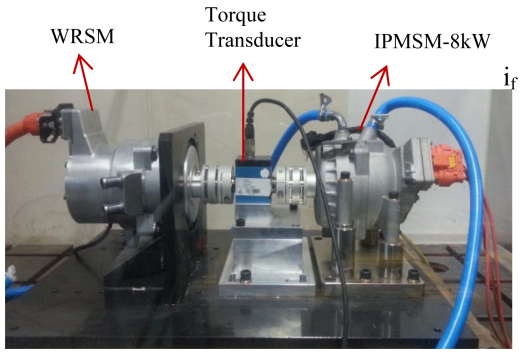

Fig. 12. (Color online) Experimental setup to test WRSM characteristics.

from 2 A to 0 A, the transition time with the chopper circuit was 100 ms, while it was 25 ms with the H-bridge. In the practice motor control, the H-bridge performed better than the chopper at reducing overvoltage of the DC bus due to EMF at high speeds. This means that the rating voltage of the three-phase main IGBT can be adopted.

3.4. Experiment of WRSM

Fig. 12 shows the experimental setup to test the WRSM characteristics. An 8 kW IPMSM was selected as the load, and speed control and torque control were executed

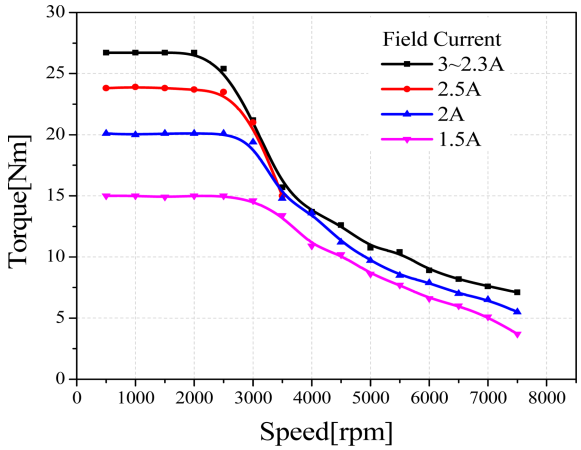

Fig. 13. (Color online) Torque characteristics according to field current.

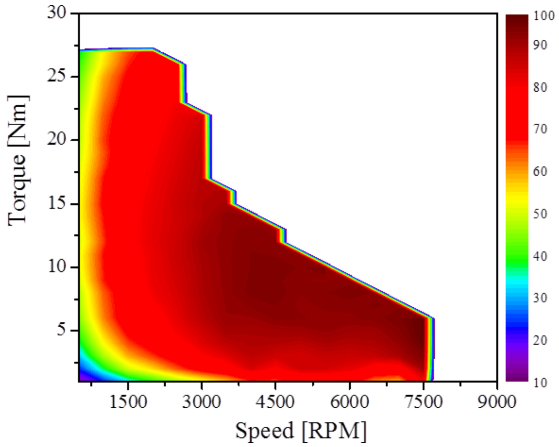

Fig. 14. (Color online) Efficiency map of WRSM prototype.

to determine the torque and power of the WRSM. A rotor excitation flux was generated via field current control by the H-bridge circuit. The maximum torque was measured according to the field current, and the result is shown in Fig. 13. Above 3000 rpm, the rotor flux was controlled by reducing the field current from 3 A to 2.3 A to maintain the maximum torque, as shown in Fig. 13. The efficiency map is shown in Fig. 14.

3.5. e-Assist Test with Combustion Engine

A developed WRSM was installed in the 900 cc combustion engine to evaluate the starting and torque assist capabilities for the belt-driven e-Assist system. Fig. 15 shows the WRSM mounted to the 900 cc combustion engine. At startup, the WRSM generated torque with the ramp function. When the engine speed was 400 rpm, fuel was injected for ignition. The WRSM stopped after ignition. Fig. 16 shows the q-axis current, phase current, and motor speed at soft startup. When the WRSM reached

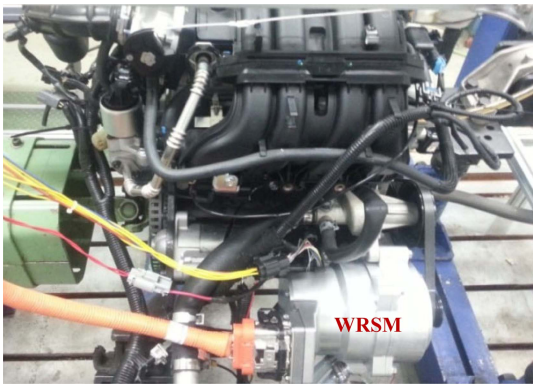

Fig. 15. (Color online) WRSM mounted to 900 cc combustion engine.

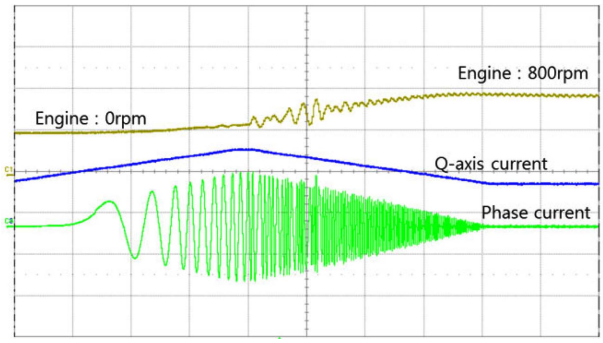

Fig. 16. (Color online) Starting characteristics of WRSM with 900 cc combustion engine [100 A/div, 200 ms/div, max 800 rpm].

1000 rpm, the q-axis current was controlled to zero. Meanwhile, fuel was supplied, and the combustion engine started instantaneously so that speed oscillation could be observed. The engine startup characteristics were improved by the WRSM torque pattern.

Fig. 17 compares engine startups with the WRSM and a

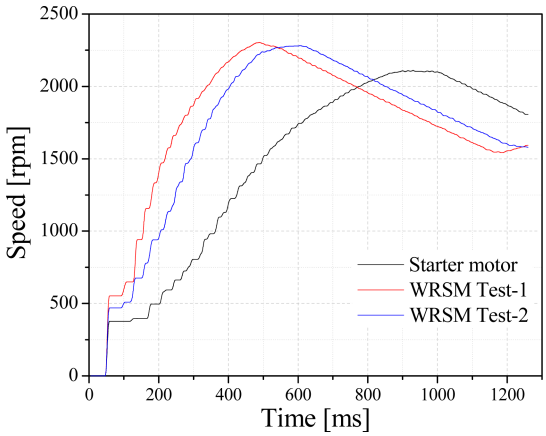

Fig. 17. (Color online) Starting test with 900 cc combustion engine.

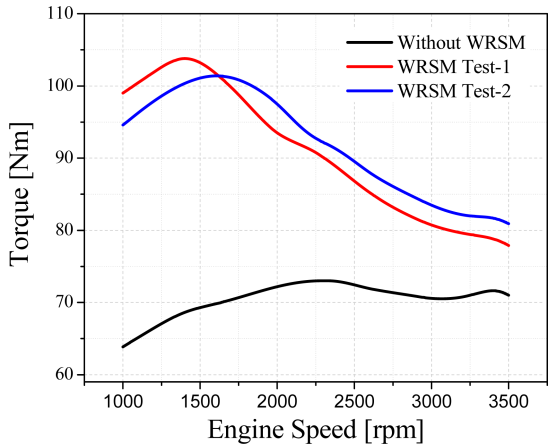

Fig. 18. (Color online) Torque assist test with 900 cc combustion engine.

conventional DC starter motor. The WRSM was tested at different pulley ratios: 2.5:1 (test 1) and 2.14:1 (test 2). The WRSM startup time of test 1 was about 50 ms shorter than that of test 2. The engine startup with WRSM was better than that with the conventional DC starter motor; thus, the idle stop and go function of BAS had good characteristics.

The e-Assist system played a critical role in increasing the automotive efficiency via motor torque assistance in the low speed region, where the engine had low efficiency. The torque assist experiment was conducted from 1000 rpm to 3500 rpm in the engine idle state. Fig. 18 depicts the torque assist characteristics at pulley ratios of 2.5:1 and 2.14:1. The experiments showed that a high torque assist can be acquired and that the system had good torque characteristics. The pulley ratio of the WRSM can be determined according to the engine efficiency test results.

4. Conclusions

In this study, a WRSM was developed for a belt-driven e-Assist system, and a prototype 115 V power electronic converter to drive the WRSM was designed and tested with a 900 cc combustion engine. The test results showed that the WRSM-type e-Assist system had good characteristics and could successfully start and assist the 900 cc combustion engine.

The field current of the WRSM could be controlled to reduce the magnetic rotor flux at high speeds with the H-bridge converter, which widened the controllable region. The H-bridge converter could adjust the field current from 2.5 A to 0 A within 25 ms, which is acceptable.

The WRSM was 20% larger than the IPMSM in volume, but it was 5% more efficient at high speeds. Therefore, the WRSM can be used as a substitute for the IPMSM in the belt-driven e-Assist system with a small increase in volume and reduced cost.

To reduce the WRSM volume as an e-Assist component, the machine needs to be designed to have a higher flux density to obtain a high starting torque. With regard to the starting torque, the rotor volume of the WRSM prototype must be increased to maximize the flux density at startup.

Acknowledgement

This work was supported by global scholarship program for foreign graduated student at Kookmin University in korea.

References

[1] G. Friedrich and A. Girardin, IEEE Ind. Appl. Mag. **12**, 26 (2009).
[2] J. E. Walters and R. J. Krefta, SAE World Congress, Mar. (2004).
[3] Geun-Ho Lee, Geo-Seung Choi, and Woong-chul Choi, JPE. **11**, 527 (2011).
[4] J. Liu, J. Hu, and L. Xu, IEEE Ind. Appl. Confer. 2754 (2004).
[5] B. W. Lee, thesis, Hanyang University (2013).
[6] Tao Sun, Ji-Min Kim, Geun-Ho Lee, Jung-Pyo Hong, and Myung-Ryul Choi, IEEE Trans. Magn. **47**, 1038 (2011).
[7] Jae-Woo Jung, Jung-Pyo Hong, and Young-Kyoun Kim, in Proc. VPPC, 778 (2007).